Semiconductor Physics, Quantum Electronics & Optoelectronics, 2023. V. 26, No 4. P. 368-375.

Semiconductor physics

Structural and morphological properties of hydroxylapatite coatings obtained by gas-detonation deposition on polymer and titanium substrates

V.P. Temchenko, V.B. Lozinskii, I.P. Vorona, O.Yo. Gudymenko, Iu.M. Nasieka*, V.M. Dzhagan, O.F. Isaieva, V.O. Yukhymchuk, M.Ya. Valakh, A.E. Belyaev

V. Lashkaryov Institute of Semiconductor Physics, NAS of Ukraine, 41, prosp. Nauky, 03680 Kyiv, Ukraine
**Corresponding author e-mail: yunaseka@gmail.com*

Abstract. The gas-detonation technique was used for the synthesis of biocompatible hydroxylapatite-based protective coatings on polymer and titanium substrates. Hydroxylapatite powder of high purity with a grain diameter of 50 μm was used as the raw material. The obtained coatings have the thickness close to 200 μm. It has been shown that the offered method enables to create of non-destructive hydroxylapatite-based coatings on polymer by varying the distance between the polymer target and the gun nozzle of gas-detonation setup. Using the data of Raman and X-ray measurements, it was ascertained that gas-detonation deposition doesn't change the composition of the deposited material. The SEM investigation testifies that the formed hydroxylapatite-based coatings are porous. EPR studies have shown that there are no paramagnetic defects in the obtained coatings, and the coating itself has a higher radiation hardness as compared to the raw powder.

Keywords: gas-detonation deposition technique, hydroxylapatite, biocompatible coating, Raman scattering, X-ray diffractometry, scanning electron microscopy, electron paramagnetic resonance.

https://doi.org/10.15407/spqeo26.04.368
PACS 07.85.Jy, 42.65.Dr, 76.30.-v, 81.15.-z

Manuscript received 13.10.23; revised version received 30.10.23; accepted for publication 22.11.23; published online 05.12.23.

1. Introduction

Great interest in the development of medical implants is due to the huge need for such products in Ukraine and in the world as a whole [1–6]. In particular, domestic medicine needs a large number of high-quality implants to restore bones damaged as a result of military actions or as a result of various diseases. Implants based on titanium and its alloys are the most widespread today. However, despite their relative biocompatibility, their implantation in the human body can cause inflammatory processes, metallosis, or even complete rejection [7]. This problem can be solved by depositing on the surface of implants biocompatible coatings, in particular, calcium phosphates (CF), such as hydroxylapatite ($Ca_{10}(PO_4)_6(OH)_2$) and calcium triphosphate ($Ca_3(PO_4)_2$), which chemical composition is close to that of bones.

Biocompatible coatings can be applied to metal implants by using various technological approaches [8–10], which have both advantages and significant disadvantages related to the low quality and high cost of the formed coatings [11, 12]. Therefore, there is a continuous search for new ways to deposit biocompatible coatings with high operational characteristics and low cost.

In this work, the method of gas-detonation deposition (GDD) was used to obtain a biocompatible hydroxylapatite (HAP) coating. The method consists in the acceleration of CF powder particles by a detonation wave that occurs as a result of an explosion taking place in the mixture of combustible gases with oxygen. CF powder particles are injected into the detonation wave, accelerated to supersonic speeds (~5M), and collated with the surface of the implant, forming a protective biotolerant coating on it.

The main advantages of the GDD method in comparison with other methods of applying protective coatings are: high adhesion, high productivity, the ability to apply layers of various thickness on implants of large areas (up to several m^2), uniformity of thickness and averaged characteristics of the coatings on different sides of the implant, the ability to vary the composition of the coating within a wide range. The low energy consumption of the GDD process defines the low cost of end products. We already tested this method for depositing HAP on titanium substrates [13, 14]. This paper presents the results of comparative studies of the structural and morphological properties of HAP coatings formed using the HDO method on polyetheretherketone

(PEEK, $C_{19}H_{14}O_3$) and titanium substrates. The choice of PEEK as a substrate was caused by good mechanical and thermoplastic properties of this polymer as well as its high inertness to aggressive environments [15, 16].

2. Experimental

HAP coatings on polymer substrates of various shapes were deposited using the setup schematically shown in Fig. 1.

As raw material for coating on polymer substrates, we used a HAP powder of high purity with a grain diameter of 50 μm. Distance from the installation gun nozzle to PEEK substrates was chosen to prevent the destruction of the polymer, when its surface was bombarded with HAP powder particles. Scanning electron microscopy (SEM), energy dispersive spectroscopy (EDA), Raman spectroscopy, X-ray diffractometry (XRD), and electron spin resonance (ESR) spectroscopy were used to characterize the prepared HAP coatings.

Raman spectra were excited using solid-state lasers with wavelength λ_{exc} of 457, 532, 671, and 785 nm, and registered using a single-stage spectrometer MDR-23 (LOMO) equipped with a cooled CCD detector Andor iDus 420 (UK). Laser power density on samples was less than 10^3 W/cm^2, to prevent any thermal modification of the samples. A spectral resolution for all excitation wavelengths did not exceed 4 cm^{-1} and was determined from the Si phonon peak width of a single crystal Si substrate. The Si phonon peak position of 520.5 cm^{-1} was used as a reference for determining the position of the peaks in the Raman spectra obtained at various λ_{exc}. XRD study was performed using Philips X'Pert PRO – MRD setup with $CuK_{\alpha l}$ line (λ = 0.15406 nm) in a symmetric (2Θ–ω) mode, with a scan step of 0.025 degrees. The voltage at the anode of the tube was 45 kV, and the current was 40 mA. The morphology of the HAP coatings was studied using Tescan Mira 3 MLU scanning electron microscope. EDS analysis was used to study the elemental composition of the HAP coatings. The ESR studies of coatings were carried out at room temperature by using Bruker ELEXSYS E580 X-band ESR spectrometer with a high-Q resonator ER4122SHQE.

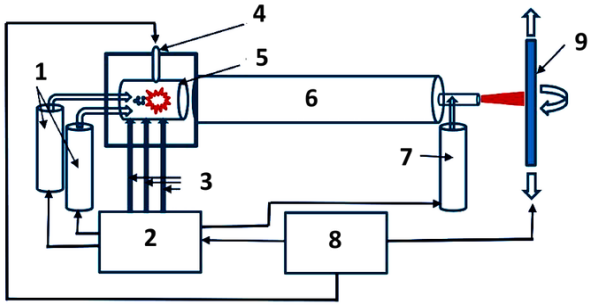

Fig. 1. Scheme of the experimental setup for GDD of HAP coatings on substrates (implants): *1*, *7* – dispensers with HAP powder, *2* – gas system, *3* – gas lines, *4* – spark plug, *5* – combustion chamber, *6* – cylinder through which the explosive wave propagates, *8* – electronic control system; *9* – substrate or implant.

3. Results and discussion

Fig. 2 shows a SEM image of formed HAP coatings on PEEK substrates (HAP/PEEK). It can be seen that the formed coatings have a porous structure with a non-uniform distribution of HAP microparticles of different sizes on the surface of the sample. With a more significant increase (Fig. 2b), 0.5…2 μm HAP flakes formed in the process of GDD are clearly observed. Such heterogeneity of the size and shape of microparticles, as well as the porosity of the HAP coatings, is a rather important positive result, since this is the structure of implant coatings that is most effective when implanting the latter into the human body.

EDA research in areas that differ in shape and size (Fig. 2c) shows that the component composition of the obtained coatings differs both among themselves and from the stoichiometric HAP (Table). For the latter, the

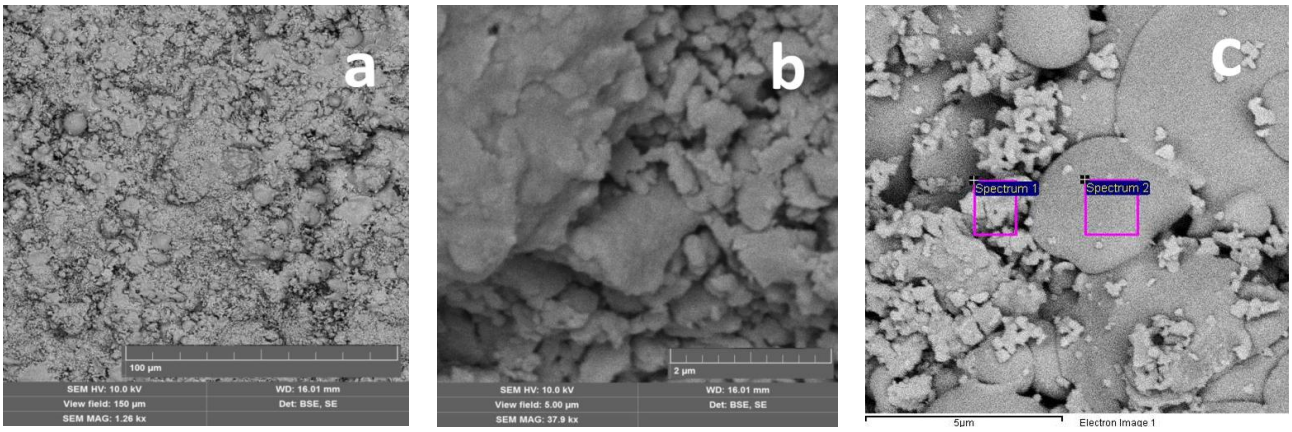

Fig. 2. SEM images of the surface of HAP coatings obtained on PEEK substrates (various magnifications). Rectangles show the areas on the sample surfaces where the component composition was analyzed with an EDA spectrometer (the obtained results are shown in Table).

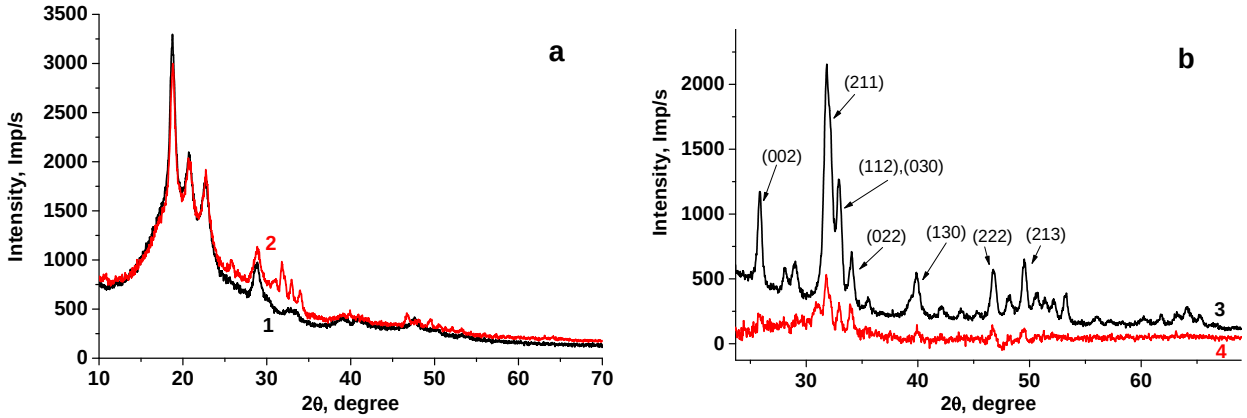

Fig. 3. X-ray diffractograms: (a) PEEK substrate (*1*) and HAP/PEEK (*2*); (b) raw HAP powder (*3*) and HAP coating obtained by subtracting curves *2* and *1* in Fig. 3a (*4*).

Ca/P ratio is 1.67, while for our samples in the area of smaller inhomogeneities (spectrum 1, Fig. 2c) Ca/P is 1.85, and in the area of flat structures (spectrum 2, Fig. 2c) this ratio is 1.81. A slightly less proportion of phosphorus in the coatings may indicate that in the process of collision of HAP particles with the substrate, their surface layer is amorphized, and for amorphous HAP the Ca/P ratio may exceed the stoichiometric and is in the range of 1.2 to 2.5 [17]. To make sure that it was the HAP coating formed in the process of GDD, their structural studies were carried out using the methods of XRD and Raman spectroscopy.

Fig. 3 shows the X-ray diffractograms of the PEEK substrate (curve *1*) and HAP/PEEK (curve *2*), in which additional diffraction peaks are observed in the region of 2Θ (30...35) and (45...50) degrees. It is obvious that the last curve is related to the contribution of both the substrate and the coating itself. To ascertain the structure of the formed coating, X-ray phase analysis of the raw powder was carried out (Fig. 3b, curve *3*), which proved that it is hydroxylapatite ($Ca_{10.00}P_{6.00}O_{26.00}H_{2.00}$) No. 96-900-2215 [18], has a hexagonal structure with the parameters $a = b = 9.4390$ nm, $c = 6.8860$ nm. Obtained as a result of subtraction of diffractograms 2 and 1 shown in Fig. 3b, curve *4* does not contain additional crystalline peaks (except for the peaks of the raw powder). This indicates that intermediate additional crystalline phases were not formed in the process of GDD, or their quantity is insignificant, and they did not appear in these studies.

Table. Elemental composition of the HAP coatings (EDA data).

	C	O	P	Ca	Total
Spectrum 1	14.68	32.79	18.44	34.09	100.00
Spectrum 2	17.44	22.91	21.23	38.42	100.00

In the Raman spectra of HAP, four main vibrational modes of the ion $(PO_4)^{3-}$ are dominant [19]: the band at 430 cm^{-1} is a doubly degenerated vibration of the O–P–O (ν_2) bend, the band at 590 cm^{-1} is a triply degenerated O–P–O bending vibrational mode (ν_4), the band at 960 cm^{-1} is fully symmetric P–O stretching vibrational mode (ν_1), and the band at 1045 cm^{-1} is a triply degenerated antisymmetric P–O stretching mode (ν_3). In the experimental Raman spectra, we observe significantly more vibrational bands, because the degenerated vibrational modes ν_2, ν_3, and ν_4 are split due to the fact that the oxygen atoms in $(PO_4)^{3-}$ occupy non-equivalent crystallographic positions.

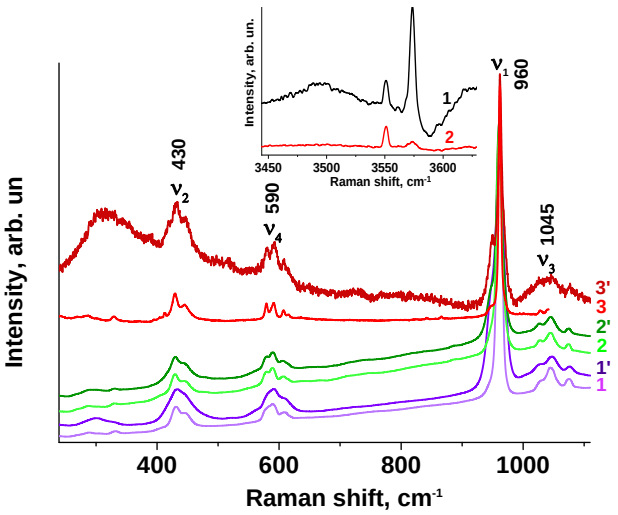

Fig. 4. Raman spectra of the HAP powder (*1*, *2*, *3*) and the coatings obtained on the titanium substrates (*1'*, *2'*, *3'*) when the spectra are excited using the laser radiation of various wavelengths: *1*, *1'* – 457 nm; *2*, *2'* – 532 nm; *3*, *3'* – 785 nm (normalized to the band intensity of 960 cm^{-1}). The inset shows the section of the spectrum in the area of OH bond oscillations: *1* – HAP powder; *2* – coating on titanium (λ_{exc} = 457 nm).

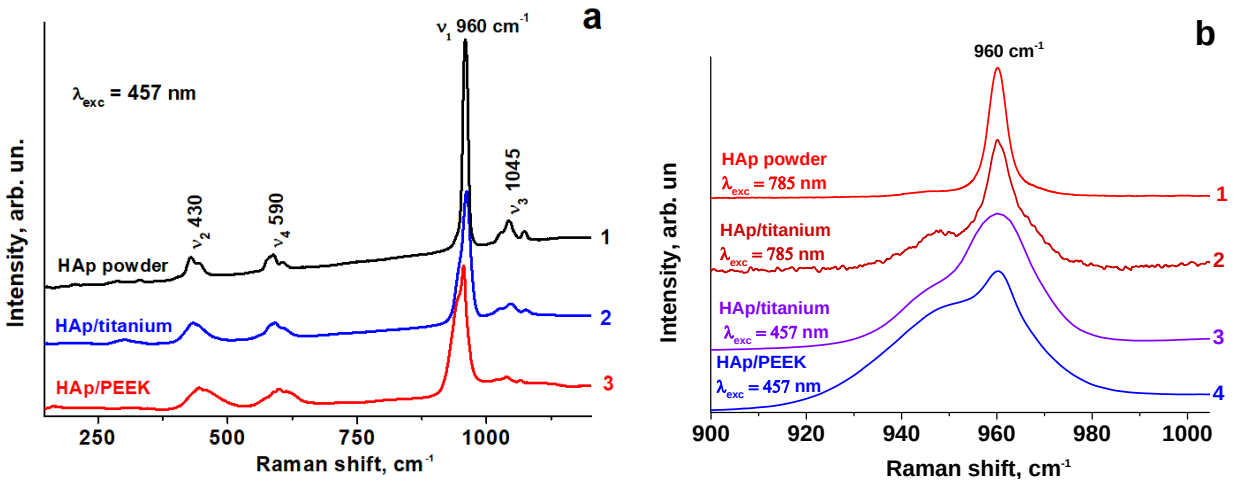

Fig. 5. (a) Raman spectra of HAP powder (*1*) and HAP coatings on titanium (*2*) and PEEK (*3*) substrates, when the spectra are excited by radiation with λ_{exc} = 457 nm; (b) Raman spectra in the region of the characteristic band of 960 cm^{-1}: HAP powder (*1*) and HAP coating on a titanium substrate (*2*), when the spectra are excited by radiation with λ_{exc} = 785 nm; coatings on titanium (*3*) and PEEK (*4*) substrates, when excited by radiation with λ_{exc} = 457 nm.

The use of laser radiation with various wavelengths enables to analyze the HAP coating at various distances from its surface, in particular, the radiation with λ = 785 nm penetrates the substrate itself and allows analyzing the transition layer formed when HAP particles were embedded into the substrate. From the analysis of the Raman spectra shown in Fig. 4, it can be stated that the crystalline perfection of HAP after its deposition onto a titanium substrate is somewhat impaired, as all the bands are broadened, which leads to their significant overlap, therefore, certain groups of bands in the spectra of the coatings look somewhat smoothed. As for the Raman spectrum obtained upon excitation by radiation with λ = 785 nm, the signal-to-noise ratio significantly deteriorates what is caused by the contribution of HAP spraying from the titanium substrate.

Fig. 5 shows the Raman spectra of the raw HAP powder and HAP coatings deposited on PEEK and titanium substrates. From Fig. 5a, it can be seen that the Raman spectra of HAP/PEEK are slightly different from the spectra of the HAP coating on a titanium substrate. The frequency positions of the Raman bands caused by the vibrational modes ν_2 and ν_4 differ from the corresponding bands of HAP coatings on titanium substrates, they are shifted to the high-frequency side. *I.e.*, the HAP coating on the polymer substrate is somewhat compressed, which led to the shift of the corresponding bands to the high-frequency side. Fig. 5b shows the Raman bands of the raw HAP powder and HAP coatings on titanium and PEEK substrates in the region where the characteristic band of ~960 cm^{-1} appears, when the spectra are excited by radiation with the wavelengths 457 and 785 nm. As expected, the symmetric band with the lowest half-width (4 cm^{-1}) is characteristic of the raw HAP powder, when the spectra are excited by radiation with λ = 785 nm.

Under the same conditions, the half-width of the band from the HAP coating on the titanium substrate is 7 cm^{-1}. It means that after deposition of HAP powder on a titanium substrate, its crystalline perfection is deteriorated, which leads to a decrease in the lifetime of phonons and, accordingly, to an increase in the half-width of the characteristic band.

The same figure shows the Raman spectra of HAP coatings formed on titanium and PEEK substrates, recorded under excitation by radiation with the wavelength 457 nm. It can be seen that for these cases the half-widths of the bands are significantly larger, which leads to their overlapping. It seems that in addition to the main mode with the frequency 960 cm^{-1}, the spectrum shows a low-frequency band with the frequency ~950 cm^{-1}, which can be attributed to amorphous HAP. Indeed, when HAP microparticles hit the substrate, their surface layer is destroyed, which can lead to partial amorphization.

This is not clearly evident in the XRD diffraction patterns due to the insignificant content of the amorphous phase. Another reason for the appearance of a band with the frequency ~950 cm^{-1} may be the transformation of HAP into tricalcium phosphate, which is characterized by a band with this frequency [20], and such a transformation was indeed observed at the temperature close to 800 °C [20]. In our case, when a microparticle of HAP powder collides with an implant, it is quite possible that the local temperature of its surface reaches this limit, at which transformation occurs. Additional confirmation of this hypothesis is provided by the Raman spectra in the region of OH bond vibrations (~3575 cm^{-1}, see inset to Fig. 4). It is known that for tricalcium phosphate the intensity of this band is significantly lower as compared to its intensity in HAP [18], which was also observed by us.

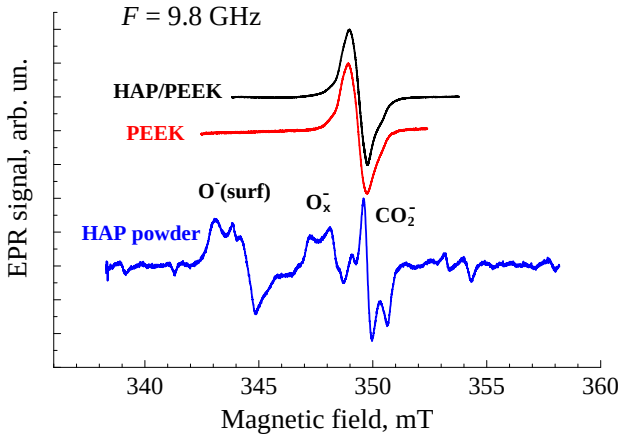

Fig. 6. ESR spectra of HAP/PEEK (*1*), pure PEEK polymer (*2*), and raw HAP powder (*3*) after electron irradiation with the dose 50 kGy.

I.e., an intense low-frequency Raman band can be caused both by partial amorphization of the surface of HAP microparticles in the process of contact with the implant, and by their partial transformation into β-tricalcium phosphate. In our case, when a microparticle of HAP powder collides with an implant, it is quite possible that the local temperature of its surface reaches this limit, at which transformation occurs. In order to detect local structure disorders of HAP particles during formation of coatings by the GDD method, studies by the ESR spectroscopy were carried out. The ESR spectrum of HAP/PEEK was a structureless symmetric line with $g \sim 2.0025$. The same ESR signal was also recorded for pure PEEK polymer. Thus, no paramagnetic defects are formed in the HAP particles during the GDD of HAP coating on PEEK substrate. On the other hand, it is known that some defects in HAP, both intrinsic and impurity, can be activated (transform into a paramagnetic state) under the action of ionizing radiation. Therefore, samples of raw HAP powder, PEEK polymer, and HAP/PEEK were irradiated with electrons at a dose of ~ 50 kGy. Their ESR spectra, normalized to the same microwave frequency, are shown in Fig. 6. The ESR spectrum of HAP/PEEK, like that of pure polymer, is a slightly asymmetric line with $g \sim 2.0040$. It is obvious that it is caused by radiation defects in the polymer.

The asymmetry of the ESR line originates from the superposition of radiation defect signals with the weaker ESR signal registered for the pure polymer. That is, we did not register ESR signals originating from the HAP. In contrast to coatings, irradiation of the raw HAP powder leads to the appearance of a complex ESR spectrum. Its analysis and comparison with the literature [21–23] allow us to single out the dominant signals from oxygen and carbon radicals (see Fig. 6). The latter testifies to the increased radiation resistance of the coatings as compared to the raw HAP powder.

4. Conclusions

Biocompatible protective coatings on polymer (PEEK) and titanium substrates with the thickness ~200 μm were prepared using gas-detonation deposition of hydroxylapatite. By varying the distance from the gun nozzle of the GDD setup to PEEK substrates, it is possible to create HAP coatings on the intact PEEK. Raman spectroscopy and X-ray diffractometry confirmed that during the HDD process of HAP powder on a PEEK substrate, a coating of precisely this compound is formed. SEM studies have enabled us to ascertain that the formed HAP coating on PEEK and titanium substrates has a porous structure. EPR studies have shown that there are no paramagnetic defects in the prepared HAP coatings, and the coating itself is more radiation resistant as compared to the original HAP powder.

Ackhowledgements

The work was carried out within the National Research Foundation of Ukraine Project No. 200/0103 "Development of the technology of biocompatible antibacterial coatings for orthopedic implants by the gas-detonation deposition method for the needs of military and civilian medicine".

References

1. Williams D.F. On the mechanisms of biocompatibility. *Biomaterials*. 2008. **29**. P. 2941–2953. https://doi.org/10.1016/j.biomaterials.2008.04.023.
2. Kuroda D., Niinomi M., Morinaga M., Kato Y., Yashiro T. Design and mechanical properties of new beta-type titanium alloys for implant materials. *Mater Sci Eng. A.* 1998. **243**. P. 244–249. https://doi.org/10.1016/S0921-5093(97)00808-3.
3. Dorozhkin S.V. There are over 60 ways to produce biocompatible calcium orthophosphate ($CaPO_4$) deposits on various substrates. *J. Compos. Sci.* 2023. **7**. P. 273. https://doi.org/10.3390/jcs7070273.
4. Koh Y.-G., Park K.-M., Lee J.-A. *et al.* Total knee arthroplasty application of polyetheretherketone and carbon-fiber-reinforced polyetheretherketone: A review. *Mater. Sci. Eng. C*. 2019. **100**. P. 70–81. https://doi.org/10.1016/j.msec.2019.02.082.
5. Furko M., Balázsi C. Calcium phosphate based bioactive ceramic layers on implant materials preparation, properties, and biological performance. *Coatings*. 2020. **10**, No 9. P. 823. https://doi.org/10.3390/coatings10090823.
6. Imamura H., Zhu W., Adachi T. *et al.* Raman analyses of laser irradiation-induced microstructural variations in synthetic hydroxyapatite and human teeth. *J. Funct. Biomater*. 2022. **13**. P. 200. https://doi.org/10.3390/jfb13040200.
7. Sasikumar Y., Indira K., Rajendran N. Surface modification methods for titanium and its alloys and their corrosion behavior in biological environment: A review. *J. Bio- Tribo-Corros*. 2019. **5**. P. 36. https://doi.org/10.1007/s40735-019-0229-5.

8. Gadow R., Killinger A., Stiegler N. Hydroxyapatite coatings for biomedical applications deposited by different thermal spray techniques. *Surf. Coat. Technol*. 2010. **205**. P. 1157–1164. https://doi.org/10.1016/j.surfcoat.2010.03.059.
9. Khor K.A., Li H., Cheang P. Significance of melt-fraction in HVOF sprayed hydroxyapatite particles, splats and coatings. *Biomaterials.* 2004. **25.** P. 1177–1186. https://doi.org/10.1016/j.biomaterials.2003.08.008.
10. Kattimani V.S., Kondaka S., Lingamaneni K.P. Hydroxyapatite – past, present, and future in bone regeneration. *Bone and Tissue Regeneration Insights*. 2016. **7**. P. 9. https://doi.org/10.4137/BTRI.S36138.
11. Simchi A., Tamjid E., Pishbin F., Boccaccini A.R. Recent progress in inorganic and composite coatings with bactericidal capability for orthopaedic applications. *Nanomedicine*. 2011. **7**. P. 22–39. http://dx.doi.org/10.1016/j.nano.2010.10.005.
12. Szcześ A., Hołysz L., Chibowski E. Synthesis of hydroxyapatite for biomedical applications. *Adv. Colloid Interface Sci.* 2017. **249**. P. 321. https://doi.org/10.1016/j.cis.2017.04.007.
13. Klyui N.I., Chornyi V.S., Zatovsky I.V. *et al.* Properties of gas detonation ceramic coatings and their effect on the osseointegration of titanium implants for bone defect replacement. *Ceram. Int.* 2021. **47**, Issue 18. P. 25425–25439. https://doi.org/10.1016/j.ceramint.2021.05.265.
14. Nosenko V.V., Yaremko A.M., Dzhagan V.M. *et al.* Nature of some features in Raman spectra of hydroxyapatite-containing materials. *J. Raman Spectroscopy*. 2016. **47**, No 6. P. 726–730. https://doi.org/10.1002/jrs.4883.
15. Haleem A., Javaid M. Polyether ether ketone (PEEK) and its 3D printed implants applications in medical field: An overview. *Clinical Epidemiology and Global Health*. 2019. **7**, Issue 4. P. 571–577. https://doi.org/10.1016/j.cegh.2019.01.003.
16. Panayotov I.V., Orti V., Cuisinier F., Yachouh J. Polyetheretherketone (PEEK) for medical applications. *Mater. Sci.: Mater. Med*. 2016. **27**. P. 118. https://doi.org/10.1007/s10856-016-5731-4.
17. Stammeier J.A., Purgstaller B., Hippler D. *et al. In-situ* Raman spectroscopy of amorphous calcium phosphate to crystalline hydroxyapatite transformation. *MethodsX*. 2018. **5**. P. 1241–1250. https://doi.org/10.1016/j.mex.2018.09.015.
18. Wilson R.M., Elliot J.C., Dowker S.E.P. Rietveld refinement of the crystallographic structure of human dental enamel apatites. *American Mineralogist*. 1999. **84**, No 9. P. 1406–1414. https://doi.org/10.2138/am-1999-0919.
19. Pezzotti G., Adachi T., Gasparutti I. *et al.* Vibrational monitor of early demineralization in tooth enamel after *in vitro* exposure to phosphoridic liquid. *Spectrochim. Acta A*. 2017. **173**. P. 19–33. https://doi.org/10.1016/j.saa.2016.08.036.
20. Bohme N., Hauke K., Dohrn M. *et al.* High-temperature phase transformations of hydroxylapatite and the formation of silicocarnotite in the hydroxylapatite–quartz–lime system studied in situ and in operando by Raman spectroscopy. *J. Mater. Sci*. 2022. **57**. 15239–15266. https://doi.org/10.1007/s10853-022-07570-5.
21. Vorona I.P., Baran N.P., Ishchenko S.S. *et al.* CO_2^- radicals in synthetic hydroxyapatite. *Phys. Solid State.* 2008. **50**. P. 1852–1856. https://doi.org/10.1134/S1063783408100119.
22. Vorona I.P., Nosenko V.V., Baran N.P. *et al.* EPR study of radiation-induced defects in carbonate-containing hydroxyapatite annealed at high temperature. *Rad. Meas.* 2016. **87**. P. 49–55. https://doi.org/10.1016/j.radmeas.2016.02.020.
23. Nosenko V., Strutynska N., Vorona I. *et al.* Structure of biocompatible coatings produced from hydroxyapatite nanoparticles by detonation spraying. *Nanoscale Res. Lett.* 2015. **10**. P. 464. https://doi.org/10.1186/s11671-015-1160-4.

Authors and CV

Volodymyr P. Temchenko, PhD, Senior Researcher at the V. Lashkaryov Institute of Semiconductor Physics. Field of interest: thin films and technologies of coatings; investigation of the influence of treatment on the properties of semiconductor materials and dielectric film, investigation of photovoltaic characteristics of solar cells, coating technologies for medical applications. E-mail: tvp@isp.kiev.ua

Volodymyr B. Lozinskii, PhD, Senior Researcher at the Department of kinetic phenomena and polaritonics, V. Lashkaryov Institute of Semiconductor Physics. Field of interest: thin films and technologies of coatings; investigation of the influence of treatment on the properties of semiconductor materials and dielectric films, investigation of photovoltaic characteristics of solar cells, coating technologies for medical applications. E-mail: Lvb60@ukr.net

Igor P. Vorona, Doctor of Physical and Mathematical Sciences in Solid State Physics (2009), Senior scientist of the Department of Optics and Spectroscopy at the V. Lashakryov Institute of Semiconductor Physics. Author of more than 90 papers. The area of his scientific interests includes EPR, ODMR and ENDOR spectroscopy, defects in solids. E-mail: vorona@isp.kiev.ua, https://orcid.org/0000-0003-1718-5569

Olexandr Yo. Gudymenko, PhD in Physics and Mathematics, Researcher at the Department of Structural and Elemental Analysis of Materials and Systems, V. Lashkaryov Institute of Semiconductor Physics. Author of more than 60 publications. His research interests include: solid-state physics, dynamical theory of diffraction of radiation, X-ray optics, X-ray diffraction analysis of semiconductor crystals, hetero- and nanosystems, XRD analysis of materials, X-ray reflectometry of thin films.
E-mail: gudymen@ukr.net,
https://orcid.org/0000-0002-5866-8084

Iurii M. Nasieka, Doctor of Sciences in Physics and Mathematics, Senior Researcher at the Department of Technology and Materials of Sensor Equipment, V. Lashkaryov Institute of Semiconductor Physics. Field of interest: materials characterization, semiconductor optics, optical materials, semiconductor detectors of ionizing radiation. Materials of interest: CdTe, CdZnTe, ZnSe, diamond coatings and films, graphite, SiO_x films.
https://orcid.org/0000-0002-3431-8856

Volodymyr M. Dzhagan, Doctor of Sciences, Professor, Leading Researcher at the V. Lashkaryov Institute of Semiconductor Physics. Authored over 180 publications. The area of scientific interests includes optical and vibrational properties of semiconductors, related nanostructures and composite materials.
E-mail: dzhagan@isp.kiev.ua,
https://orcid.org/0000-0002-7839-9862

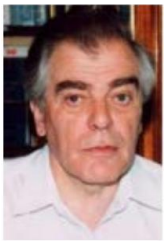

Mykhailo Ya. Valakh, defended his Dr. Sci. thesis in 1982 and received the academic title of Professor in 1985, all in the Institute of Semiconductor Physics, National Academy of Sciences of Ukraine. To-date he is the Main scientist in the Optical Department of the V. Lashkaryov Institute of Semiconductor Physics. He is the author of more than 400 scientific publications with h = 35 (Scholar Google), 7 patents, 5 textbooks. The area of his scientific interests includes physics of semiconductors and dielectrics, optics and spectroscopy of solid state, materials science for electronics, physics of nanostructures, optical diagnostics of materials.
E-mail: mvalakh@gmail.com,
https://orcid.org/0000-0003-3849-3499

Oksana Isaieva, born in 1994, PhD in Applied Physics and Nanomaterials (2021), Researcher at the Department of optics and spectroscopy, V. Lashkaryov Institute of Semiconductor Physics. Author of 14 publications, which are included in the Scopus, 6 patents. The area of her scientific interests includes nano-nanocomposites and their synthesis, optical properties of nanomaterials. E-mail: oksanka.isayeva@gmail.com,
https://orcid.org/0000-0003-1313-5409

Volodymyr O. Yukhymchuk, Professor, Doctor of Sciences in Physics and Mathematics, Head of the Department at the V. Lashkaryov Institute of Semiconductor Physics. The area of his scientific interests includes Raman spectroscopy, luminescence, quantum dots, semiconductors, nanostructures.
E-mail: v.yukhymchuk@gmail.com,
https://orcid.org/0000-0002-5218-9154

Alexander Belyaev, Professor, Academician of NAS of Ukraine. He obtained PhD degree in semiconductor physics and dielectrics in 1980, the Dr. Sc. degree in 1991. A. Belyaev is Professor from 1999. He is the author of more than 220 publications. The area of his scientific researches is transport and optical properties in quantum multi-layer heterostructures and low-dimensional systems as well as their application in UHF devices. E-mail: belyaev@isp.kiev.ua,
https://orcid.org/0000-0001-9639-6625

Authors' contributions

Temchenko V.P.: synthesis and treatment of hydroxylapatite coatings.
Lozinskii V.B.: synthesis and treatment of hydroxylapatite coatings.
Vorona I.P.: investigation, resources, data analysis, writing – original draft.
Gudymenko O.Yo.: investigation, resources, data analysis, writing – original draft.
Nasieka Iu.M.: data analysis, writing – original draft.
Dzhagan V.M.: methodology, writing – original draft.
Isaieva O.F.: Raman measurements, data analysis.
Yukhymchuk V.O.: conceptualization, supervision, writing – review and editing.
Valakh M.Ya.: conceptualization, supervision, writing – review and editing.
Belyaev A.E.: conceptualization (lead); funding acquisition (lead); resources (lead); supervision (lead); writing – review & editing (equal).

Структурні і морфологічні властивості гідроксилапатитних покриттів, отриманих методом газодетонаційного осадження на полімерних та титанових підкладках

В.П. Темченко, В.Б. Лозінський, І.П. Ворона, О.Й. Гудименко, Ю.М. Насєка, В.М. Джаган, О.Ф. Ісаєва, В.О. Юхимчук, М.Я. Валах, О.Є. Бєляєв

Анотація. Метод газодетонаційного осадження використано для осадження біосумісних гідроксилапатитних (ГАП) захисних покриттів на полімерні і титанові підкладки. Як вихідний матеріал використано високочистий порошок гідроксилапатиту з фракцією 50 мкм. Отримані ГАП покриття мали товщину ~ 200 мкм. Показано, що змінюючи відстань від полімерної мішені до сопла «гармати» газодетонаційної установки, можна отримати ГАП покриття без руйнування самого полімеру. Методами комбінаційного розсіювання світла і Х-променевої дифрактометрії встановлено, що процес газодетонаційного осадження не змінює компонентного складу вихідного порошку. Дослідження сформованих ГАП покриттів методом скануючої електронною мікроскопією показали, що отримані покриття є пористими. Методом електронного парамагнітного резонансу показано відсутність парамагнітних дефектів в отриманих покриттях, останні виявились більш радіаційно-стійкими у порівнянні з вихідним порошком.

Ключові слова: газодетонаційне осадження, гідроксилапатит, біосумісне покриття, комбінаційне розсіювання світла, Х-променева дифрактометрія, скануюча електронна мікроскопія, електронний парамагнітний резонанс.